Turkish Journal of Electrical Engineering & Computer Sciences

http://journals.tubitak.gov.tr/elektrik/

Research Article

Turk J Elec Eng & Comp Sci
(2015) 23: 1558 – 1570

doi:10.3906/elk-1402-120

A novel control method for a VSC-HVDC system in a grid-connected wind farm

Yingpei LIU*, Ran LI
School of Electrical & Electronic Engineering, North China Electric Power University, Baoding, P.R. China

Received: 12.02.2014 • **Accepted/Published Online:** 05.07.2014 • **Printed:** 30.11.2015

Abstract: The voltage source converter-high voltage direct current (VSC-HVDC) transmission is the ideal integration technology for grid-connected wind farms. A passivity-based control (PBC) method for VSC-HVDC when the wind farm voltage is unbalanced is proposed in this paper. The mathematical model of a VSC with unbalanced voltage is established. The PBC theory including dissipation inequality and system strict passivity is introduced, and then the stability of PBC is proven in light of the Lyapunov stability theory. According to PBC theory, a Euler–Lagrange mathematical model of a VSC is constructed. After that, the strict passivity of the VSC is proven. On the premise of the power factor being 1, the PBC controller for the VSC-HVDC system is designed under d-q coordination. The control law is deduced in detail. In order to accelerate the convergence speed, dampers are added to the PBC controller. The decoupled control of the active power and the reactive power is achieved by this method. The dynamic and steady performances of the VSC-HVDC system in a grid-connected wind farm when the wind farm voltage is unbalanced are significantly improved. Furthermore, the robustness of the system is enhanced. The simulation results verify the feasibility and correctness of the method.

Key words: Grid-connected wind farm, voltage source converter-high voltage direct current, passivity-based control, unbalanced voltage

1. Introduction

Wind energy resource distribution is an important regional issue. Furthermore, the rich regions with abundant wind energy resources are often far away from the load centers. Therefore, a wind farm connected to the power grid must go through long-distance transmission [1,2]. To ensure good economics and stability, how to connect the wind farm to the power grid has become the focus of scholars' study.

Voltage source converter-high voltage direct current (VSC-HVDC) technology is a new generation of HVDC transmission technology based on VSC and purse width modulation (PWM) technologies. VSC-HVDC technology has high flexibility and controllability, which can simultaneously provide the active power and the reactive power support to the system. The stability and transmission capability of a power system can be significantly improved using VSC-HVDC technology. The voltage level of the point of common coupling is stable. VSC-HVDC is the ideal transmission for large wind farms connected to a power grid.

Currently, many studies on VSC-HVDC control strategies have been published, but most are based on ideal conditions with AC voltage balanced [3–9]. The control strategy for VSC-HVDC when AC power is unbalanced is researched less often. However, the AC voltage is not entirely balanced, and short circuit faults and break line faults are inevitable. In the grid-connected wind farm, when the wind farm voltage is unbalanced, the

*Correspondence: liuyingpei_123@126.com

VSC-HVDC system controller built under balance voltage will not be able to maintain system stability control requirements; the stable operation ability of the VSC is also seriously affected, which results in bad output voltage quality. Furthermore, direct current voltage fluctuation causes transmitted power fluctuation, which will affect the stability of the entire system through the transmission lines. Therefore, it is necessary to study VSC-HVDC system control strategy with unbalanced wind farm voltage, aiming at improving VSC-HVDC system performance when AC voltage is unbalanced.

The VSC control strategy directly impacts VSC-HVDC performance. Traditionally, a PI controller is used in double closed-loop control. Although a PI controller has a simple structure, it has some flaws; for example, its robustness to parameters is poor. Therefore, it does not meet high performance requirements. On the contrary, the passivity-based control (PBC) theory has shown superior control performance. From the point of view of energy, PBC theory seeks the energy function related to the controlled variable. With the designed passive controller, the energy function tracks the expected energy function so as to achieve control objective. In detail, the reactive component in the energy dissipation characteristic equation of the system is configured in order to force the system's total energy to track the expected energy function. Therefore, the stability of the system is ensured, the system state variables asymptotically converge to their set values, and the outputs of the controlled object asymptotically converge to the desired values. Compared to the linearization control method, the superiority of the PBC method lies in the designed passive controller, which focuses on the natural properties of the object. Accordingly, the robustness of the system is effectively improved. The control law designed for PBC ensures that the system is globally stable with no divergent singular point.

A 4-dimensional hyperchaotic system based on PBC strategies is realized here. First, a periodically intermittent controller is used to stabilize the system states to equilibrium and to achieve the projective synchronization of the system, in both its periodic and hyperchaotic regimes. Then, based on the stability properties of a passive system, a linear passive controller is designed to drive the system trajectories asymptotically to the origin, which only requires the knowledge of the system output [10]. The control of a passive plant utilizing strictly passive feedback as motivated by the passivity theorem is studied. The theoretical results in the study are applied to a number of application examples, demonstrating that a much broader class of controllers can deliver closed-loop global stability and asymptotic convergence [11]. For the high-performance torque tracking and the flux observer of the induction motors, a passivity-based tracking controller and adaptive observer are proposed. An adaptive controller is developed based on the Lyapunov stability theory to realize the online estimation of the flux magnitude, motor speed, and stator resistance. Simulation results show that the proposed adaptive-observer-based passivity tracking control strategy can effectively improve the static and dynamic performances of the induction motors [12,13]. The PBC method is also successfully used for permanent magnet linear synchronous motors [14] and permanent magnet synchronous motors [15].

In this paper, a passivity-based control method for VSC-HVDC in a grid-connected wind farm when the wind farm voltage is unbalanced is put forward. The VSC mathematical model under unbalanced voltage is established. On this basis, a VSC Euler–Lagrange (EL) mathematical model is constructed. The strict passivity of VSC is proven. On the premise of the power factor being 1, the PBC controller for the VSC-HVDC system is designed under d, q coordination. The control law is deduced in detail. In order to accelerate the convergence rate, dampers are added to the PBC controller. The decoupled control of the active power and the reactive power is achieved by this method. The dynamic and steady performances of the VSC-HVDC system when the wind farm voltage is unbalanced are significantly improved.

2. The VSC mathematical model under unbalanced power grid voltage

The main circuit topology of VSC in which a 3-phase-bridge circuit is adopted is shown in Figure 1, where, e_a, e_b, e_c are the 3-phase voltages of the wind farm; i_a, i_b, i_c are the 3-phase currents; u_{DC} is the DC voltage; R is the equivalent resistance between the wind farm and the VSC; L is the equivalent inductance between the wind farm and the VSC; C is the DC-link capacitor; i_L is the load current; and N is the neutral point of the power grid.

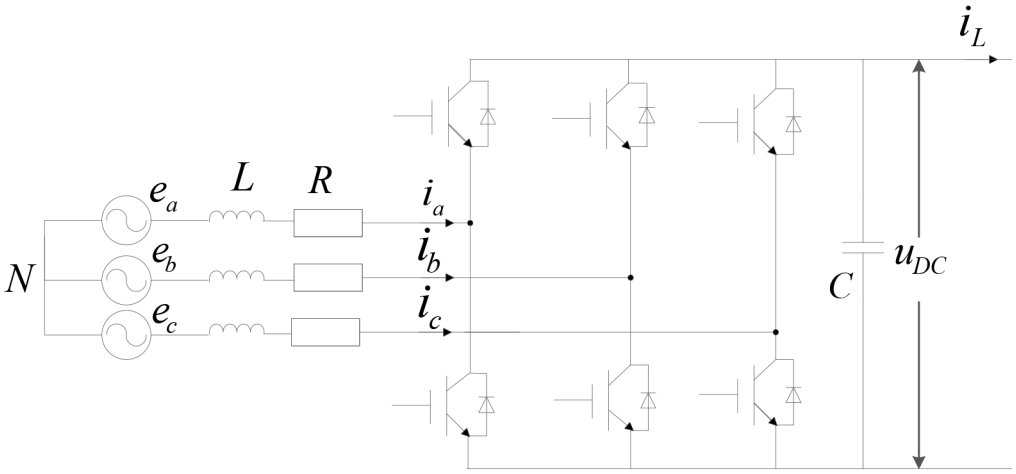

Figure 1. The main circuit topology of VSC.

From Figure 1, when the wind farm voltage is unbalanced, the values of e_a, e_b, e_c and i_a, i_b, i_c are shown by Eq. (1).

$$\begin{cases} e_a + e_b + e_c \neq 0 \\ i_a + i_b + i_c = 0 \end{cases} \tag{1}$$

The mathematical model of VSC is shown in Eq. (2).

$$\begin{cases} L\frac{di_a}{dt} = e_a - Ri_a - (s_a u_{DC} + u_{ON}) \\ L\frac{di_b}{dt} = e_b - Ri_b - (s_b u_{DC} + u_{ON}) \\ L\frac{di_c}{dt} = e_c - Ri_c - (s_c u_{DC} + u_{ON}) \\ C\frac{du_{DC}}{dt} = i_a s_a + i_b s_b + i_c s_C - i_L) \end{cases} \tag{2}$$

In Eq. (2), s_a, s_b, s_c are the switching functions of VSC, which are defined as follows: $s_j (j = a, b, c) = 1$ when the upper bridge arm turns on and $s_j = 0$ when the lower bridge arm turns on; u_{ON} is the common point voltage of the lower bridge arm.

Eq. (3) is derived according to Eqs. (1) and (2).

$$u_{ON} = \frac{1}{3}[e_a + e_b + e_c - (s_a + s_b + s_c)u_{DC}] \tag{3}$$

Eq. (3) is substituted into Eq. (2), and then the mathematical model of VSC with unbalanced AC voltage is obtained as shown in Eq. (4).

$$\begin{cases} L\frac{di_a}{dt} = e_a - \frac{1}{3}(e_a+e_b+e_c) - Ri_a - (\frac{2s_a-s_b-s_c}{3})u_{DC} \\ L\frac{di_b}{dt} = e_b - \frac{1}{3}(e_a+e_b+e_c) - Ri_b - (\frac{2s_b-s_a-s_c}{3})u_{DC} \\ L\frac{di_a}{dt} = e_c - \frac{1}{3}(e_a+e_b+e_c) - Ri_c - (\frac{2s_c-s_b-s_a}{3})u_{DC} \\ C\frac{du_{DC}}{dt} = i_a s_a + i_b s_b + i_c s_C - i_L \end{cases} \tag{4}$$

Through the 2-phase synchronous rotating d,q transformation, the mathematical model of VSC with unbalanced AC voltage in a synchronous rotating reference frame is represented in Eq. (5).

$$\begin{cases} L\frac{di_d}{dt} = u_d - Ri_d + \omega L i_q - s_d u_{DC} \\ L\frac{di_q}{dt} = u_q - Ri_q - \omega L i_d - s_q u_{DC} \\ \frac{2}{3}C\frac{du_{DC}}{dt} = s_d i_d + s_q i_q - \frac{2}{3}i_L \end{cases} \tag{5}$$

In Eq. (5), u_d, u_q are the d,q components of e_a, e_b, e_c respectively; i_d, i_q are the d,q components of i_a, i_b, i_c respectively; and s_d, s_q are the d,q components of s_a, s_b, s_c.

3. The theory of PBC and its stability proof

3.1. The theory of PBC

Consider the nonlinear system

$$\begin{cases} \dot{x} = f(x,u) \\ y = h(x) \end{cases}, \tag{6}$$

where $x \in R^n, u \in R^m$.

Assume $f(0,0) = 0$. There exists a continuously differentiable and positive semidefinite function $V(x)$, which is called storage function, such that

$$V(x(t)) - V(x(0)) \le \int_0^T u^T y dt. \tag{7}$$

Eq. (7) is the dissipation inequality. From Eq. (7), it can be seen that the sum of system energy growth is always less than the sum of external injection energy. That is to say that the operation of the system of Eq. (6) is always accompanied by loss of energy.

If there exist a positive semidefinite storage function $V(x)$ and a positive function $Q(x)$, such that $\forall T > 0$,

$$V(x(T) - V(x(0) \le \int_0^T u^T y dt - \int_0^T Q(x) dt, \tag{8}$$

or

$$\dot{V} \le u^T y - Q(x), \tag{9}$$

then the system of Eq. (6) is strictly passive. From the above, it can be seen that passivity is closely related to the input and output of the system.

3.2. The stability proof of PBC

Considering the strictly passive system of Eq. (6), there exists a continuously differentiable storage function $V(x)$ that satisfies Eq. (9). Considering $u = 0, \forall t \geq 0$, we can then get Eq. (10).

$$\dot{V} \leq -Q(x) < 0, \qquad \forall t \geq 0 \tag{10}$$

Eq. (10) indicates that the strictly passive system of Eq. (6) meets the Lyapunov stability condition. Then $x = 0$ is the asymptotic stability of the equilibrium point, and $V(x)$ is the Lyapunov function.

3.3. The EL mathematical model of the passive system

The EL mathematical equation of the passive system of Eq. (6) is shown in Eq. (11).

$$M\dot{x} + Cx + Rx = u \tag{11}$$

In Eq. (11), M is a diagonal positive matrix, C is an antisymmetric matrix, R is a symmetric positive matrix, and u is the input of the system.

The energy function is chosen as

$$V = \frac{1}{2}x^T W x, \tag{12}$$

where $W = MR^{-1}M$ is a positive symmetric matrix.

Then,

$$\dot{V} = x^T MR^{-1}u - x^T Nx - x^T Mx, \tag{13}$$

where $N = MR^{-1}C$is a symmetric matrix.

Thus,$x^T Nx = 0$. Eq. (14) is obtained from Eq. (13).

$$\dot{V} = x^T MR^{-1}u - x^T Mx \tag{14}$$

In Eq. (14), we choose $Q(x) = x^T Mx$. Because $M$is a diagonal positive matrix, $Q(x) > 0$. Define$y^T = x^T MR^{-1}$, and then through integral transformation for Eq. (14), Eq. (15) can be obtained.

$$V(x(t)) - V(x(0)) \leq \int_0^T uy^T dt - \int_0^T Q(x)dt \tag{15}$$

From Eq. (15), we can see that the system of Eq. (6) as described by Eq. (11) is strictly passive, and $x = 0$is the asymptotic stability of the equilibrium point.

4. Design of PBC controller for VSC-HVDC system

4.1. The passivity verification of VSC

Eq. (16) is transformed from Eq. (5).

$$\begin{pmatrix} L & 0 & 0 \\ 0 & L & 0 \\ 0 & 0 & \frac{2}{3}C \end{pmatrix} \begin{pmatrix} L\frac{di_d}{dt} \\ L\frac{di_q}{dt} \\ \frac{du_{DC}}{dt} \end{pmatrix} + \begin{pmatrix} 0 & -\omega L & s_d \\ \omega L & 0 & s_q \\ -s_d & -s_q & 0 \end{pmatrix} \begin{pmatrix} i_d \\ i_q \\ u_{DC} \end{pmatrix} + \begin{pmatrix} R & 0 & 0 \\ 0 & R & 0 \\ 0 & 0 & \frac{2}{3R_L} \end{pmatrix} \begin{pmatrix} i_d \\ i_q \\ u_{DC} \end{pmatrix} = \begin{pmatrix} u_d \\ u_q \\ 0 \end{pmatrix} \tag{16}$$

In Eq. (16), $R_L=\frac{u_{DC}}{i_L}$, R_L is the equivalent resistance of the DC link.

The EL model of VSC shown in Eq. (17) is obtained from Eq. (16).

$$M\dot{x}+Jx+Rx=u \tag{17}$$

In Eq. (17), M is a diagonal positive matrix; R is a symmetric positive matrix; J is an antisymmetric matrix; $M=\begin{pmatrix} L & 0 & 0 \\ 0 & L & 0 \\ 0 & 0 & \frac{2}{3}C \end{pmatrix}; x=\begin{pmatrix} x_1 \\ x_2 \\ x_3 \end{pmatrix}=\begin{pmatrix} i_d \\ i_q \\ u_{DC} \end{pmatrix}; J=\begin{pmatrix} 0 & -\omega L & s_d \\ \omega L & 0 & s_q \\ -s_d & -s_q & 0 \end{pmatrix}; R=\begin{pmatrix} R & 0 & 0 \\ 0 & R & 0 \\ 0 & 0 & \frac{2}{3R_L} \end{pmatrix}$; and $u=\begin{pmatrix} u_d \\ u_q \\ 0 \end{pmatrix}$.

The energy function of VSC $V_1=\frac{1}{2}x^TMx$ is chosen. Eq. (18) is calculated by differentiation operation of V_1 and then substitution of Eq. (17) into it.

$$\dot{V}_1=x^TM\dot{x}=x^T(u-Jx-Rx) \tag{18}$$

In Eq. (18), since J is an antisymmetric matrix, $x^TJx=0$.

Therefore, Eq. (19) is obtained.

$$\dot{V}_1=x^Tu-x^TRx \tag{19}$$

According to Eq. (19), we now define $y=x$ and $Q(x)=x^TRx$, and then $\dot{V}_1\le u^Ty-Q(x)$. Considering that $Q(x)$ is a positive function, Eq. (19) accordingly meets the dissipation inequality, which means that VSC is strictly passive. Thus, PBC theory can be applied to VSC.

4.2. Design of PBC controller

The power factor is expected to be 1 in the VSC-HVDC system; therefore, we have the expected state variables values, which are $x_1^*=i_d^*\,x_2^*=i_q^*=0\,x_3^*=u_{DC}^*$. Here, i_d^* is the expected value of i_d; i_q^* is the expected value of i_q and the power factor is 1, so $i_q^*=0$; u_{DC}^* is the expected value of u_{DC}.

Define the state error $x_e=x-x^*$. Eq. (20) is then calculated from Eq. (17).

$$M\dot{x}_e+Jx_e+Rx_e=u-M\dot{x}^*-Jx^*-Rx^* \tag{20}$$

The error energy function V_2 is chosen as shown in Eq. (21).

$$V_2=\frac{1}{2}x_e^TMx_e \tag{21}$$

Eq. (22) is then calculated by differentiation operation of V_2 and then substitution of Eq. (17) into it.

$$\dot{V}_2=x_e^TM\dot{x}_e=x_e^T(u-M\dot{x}^*-J(x^*+x_e)-R(x^*+x_e)) \tag{22}$$

The control law is set as in Eq. (23).

$$u=M\dot{x}^*+J(x^*+x_e)+Rx^* \tag{23}$$

We then substitute Eq. (23) into Eq. (22). Eq. (24) is obtained.

$$\dot{V}_2 = -x_e^T R x_e < 0 \tag{24}$$

Considering $M\dot{x}^* = 0$, from Eq. (23), the control law is obtained in detail as shown in Eq. (25).

$$\begin{cases} s_d = \frac{u_d + \omega L i_q - R i_d^*}{u_{DC}} \\ s_q = \frac{u_q - \omega L i_d}{u_{DC}} \end{cases} \tag{25}$$

In order to analyze the performance of the designed PBC controller, we substitute Eq. (25) into Eq. (5). Eq. (26) is derived.

$$\begin{cases} \frac{L}{R}\frac{di_d}{dt} + i_d = i_d^* \\ \frac{L}{R}\frac{di_q}{dt} + i_q = 0 \end{cases} \tag{26}$$

It can be seen from Eq. (26) that the value of time constant $L/R$is small; therefore, $i_d$can converge to i_d^* quickly and i_q converges to $i_q^* = 0$. Because i_d, i_q respectively represent the active current component and reactive current component, according to Eq. (26), the decoupled control of the active power and reactive power through the PBC controller for the VSC-HVDC system is achieved.

In order to accelerate the convergence speed, dampers are added to the PBC controller. Define Eq. (27):

$$R_d x_e = (R + R_a) x_e, \tag{27}$$

where $R_a = \begin{pmatrix} R_{a1} & 0 & 0 \\ 0 & R_{a2} & 0 \\ 0 & 0 & 0 \end{pmatrix}$; $R_{a1}, R_{a2}$are the damper values; and $R_d$is a positive symmetric matrix.

Thus, Eq. (28) is derived with dampers considered.

$$M\dot{x}_e + Jx_e + Rx_e + R_a x_e = u - M\dot{x}^* - Jx^* - Rx^* + R_a x_e \tag{28}$$

Eq. (29) is obtained by simplifying Eq. (28).

$$M\dot{x}_e + R_d x_e = u - (M\dot{x}^* + J(x^* + x_e) + Rx^* - R_a x_e) \tag{29}$$

With dampers considered, the control law is chosen as shown in Eq. (30).

$$u = M\dot{x}^* + J(x^* + x_e) + Rx^* - R_a x_e \tag{30}$$

We then substitute Eq. (30) into Eq. (29). Eq. (31) is obtained.

$$M\dot{x}_e = -R_d x_e \tag{31}$$

The error energy function considering the dampers $V_3 = \frac{1}{2} x_e^T M x_e$ is chosen. $\dot{V}_3 = x_e^T M \dot{x}_e = -x_e^T R_d x_e = -x_e^T (R + R_a) x_e < 0$ can be easily obtained. Therefore, it can be seen that the convergence speed becomes faster.

From Eq. (30), the new control law with dampers is shown in Eq. (32).

$$\begin{cases} S_d = \frac{u_d+\omega L i_q - R i_d^* + R_{a1}(i_d - i_d^*)}{u_{DC}} \\ S_q = \frac{u_q - \omega L i_d + R_{a2} i_q}{u_{DC}} \end{cases} \tag{32}$$

In order to analyze the performance of the designed PBC controller of Eq. (32), we substitute Eq. (32) into Eq. (5). Eq. (33) is derived.

$$\begin{cases} \frac{L}{R+R_{a1}} \frac{di_d}{dt} + i_d = i_d^* \\ \frac{L}{R+R_{a2}} \frac{di_q}{dt} + i_q = 0 \end{cases} \tag{33}$$

It can be seen from Eq. (33) that if the values of R_{a1}, R_{a2} are large, i_d can track and converge to i_d^* quickly and i_q tracks and converges to $i_q^* = 0$.

The VSC-HVDC system based on the PBC method in a grid-connected wind farm is shown in Figure 2. The system consists of the wind farm, 2 convertors with their control systems (the first is a rectifier and the other is an inverter), the DC link, and the power grid. In the VSC-HVDC system, constant DC voltage control and constant reactive power control are applied to the convertor. The working process is as below. The DC voltage error is calculated by subtracting the given value of DC voltage u_{DC}^* from the actual value of DC voltage u_{DC}. The PI regulator outputs i_d^* with the DC voltage error as the input signal. In order to achieve a power factor of 1, the given reactive power Q^* is set to 0. Another PI regulator outputs i_q^* with the reactive power error by subtracting Q^* from the actual value Q as the input signal. e_a, e_b, e_c and i_a, i_b, i_c are captured in real time from the wind farm and VSC-HVDC system. Then, u_d, u_q and i_d, i_q are obtained from abc/dq transformation. With the input signals of $u_d, u_q, i_d, i_q, i_d^*, i_q^*$, and u_{DC}, the PBC controller computes the output signals according to Eq. (32), which is afterwards modulated by space-vector PWM into 6 pulses to control the VSC operation. The decoupled control of the active power and the reactive power is achieved.

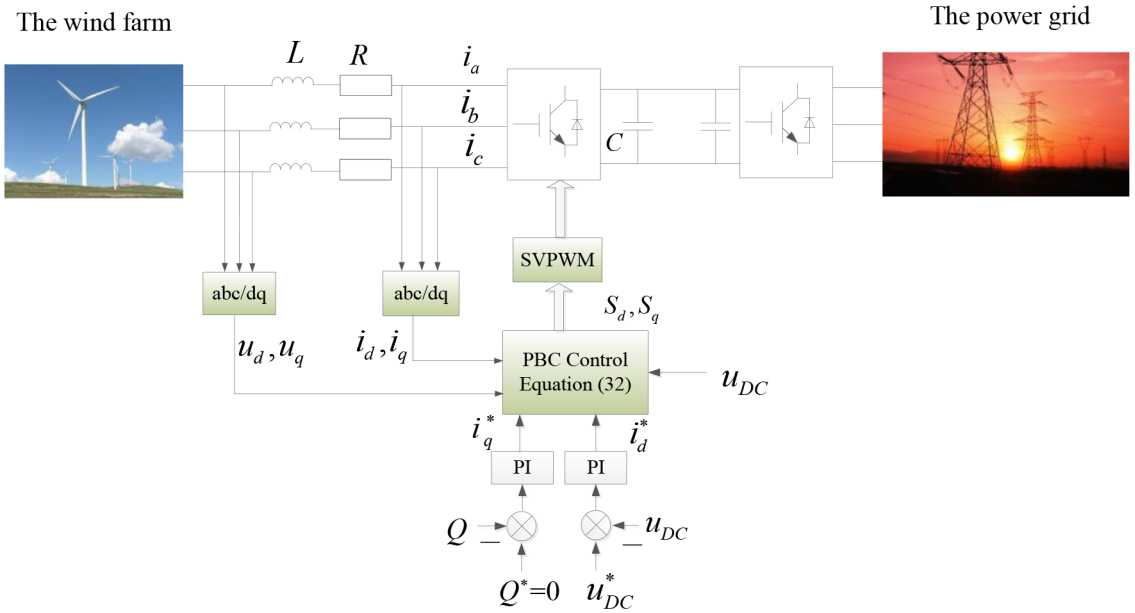

Figure 2. The diagram of the VSC-HVDC system based on PBC method in grid-connected wind farm.

5. Simulation results

The simulation model of the VSC-HVDC system based on PBC method as shown in Figure 3 is constructed based on MATLAB/SIMULINK, including the power grid model, the PBC controller model, the PWM model and the related signal calculation model, and so on. The wind farm is represented as a 3-phase source. The PBC controller simulation submodel is shown in Figure 4. The signal calculation simulation submodel is shown in Figure 5. The main parameters of the VSC-HVDC system are shown in the Table.

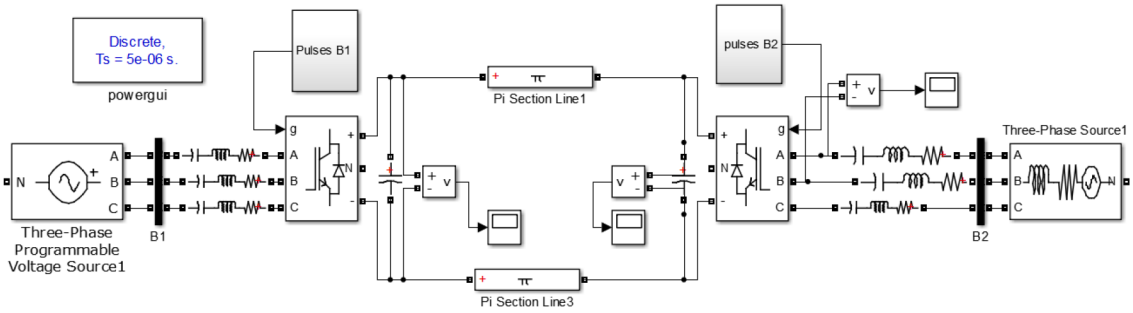

Figure 3. The simulation model of the VSC-HVDC system based on PBC method.

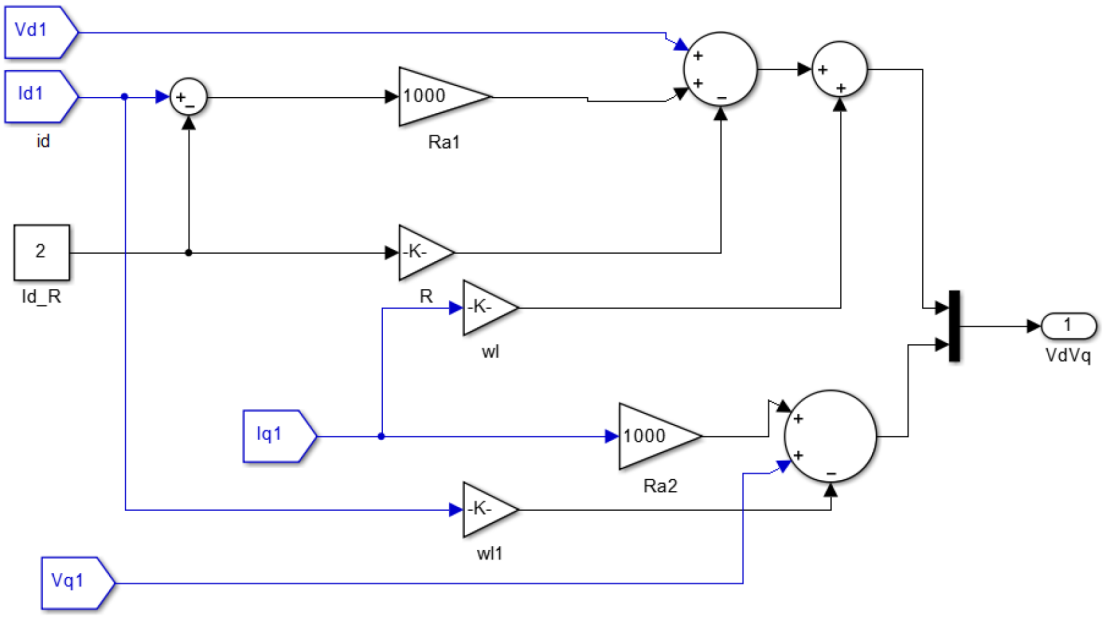

Figure 4. The PBC controller simulation submodel.

Table. The main parameters of the VSC-HVDC system.

The parameters	The parameter values
The power grid phase voltage	35 kV
The equivalent inductance between the power grid and the VSC	L= 33.36 mH
The equivalent resistance between the power grid and the VSC	R= 0.1 .Ω
The DC line length	10 km
The DC-link capacitor	4700 μF

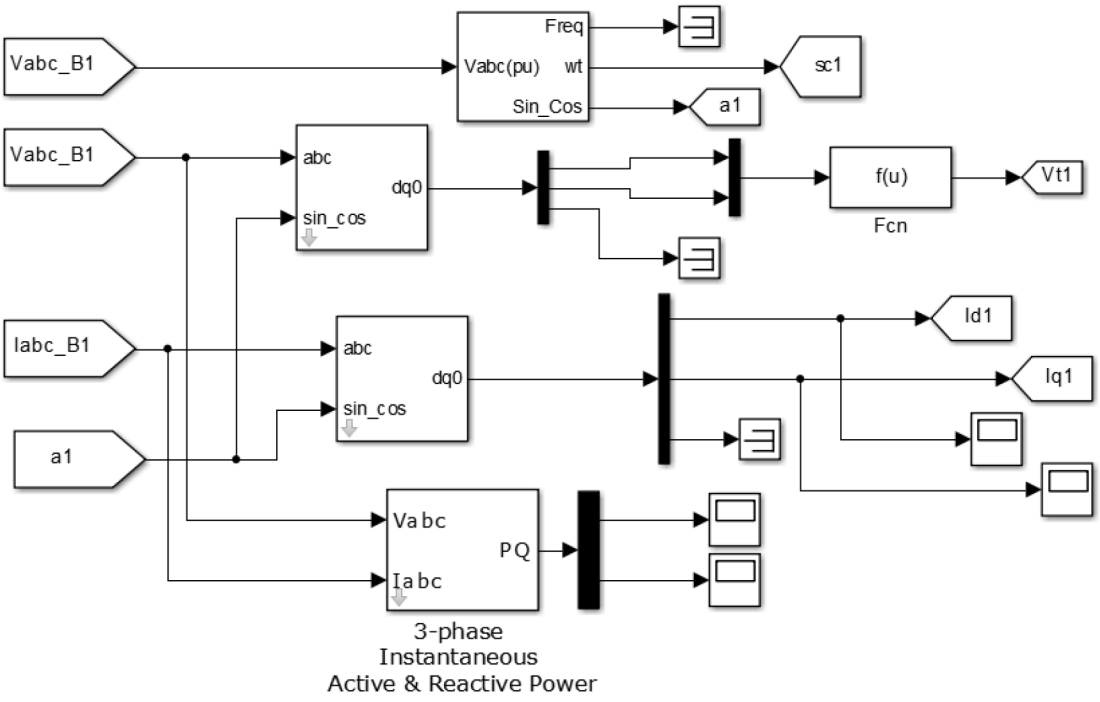

Figure 5. The signal calculation simulation submodel.

The reference voltage of the wind farm is chosen for 35 kV. The reference capacity is chosen for 100 MW. $u^*_{DC} = 3 \times 10^5 V$. The VSC-HVDC system runs when the wind farm voltage unbalances at 0.5 s and then it recovers to balance at 0.6 s. Under this condition, the wind farm voltage waves are shown in Figure 6. The VSC-HVDC system simulation waves under the PI method are shown in Figure 7. The VSC-HVDC system simulation waves under the PBC method are shown in Figure 8.

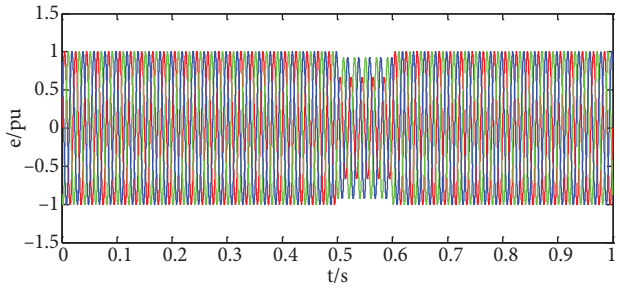

Figure 6. The wind farm voltage waves (per unit).

From Figure 6, we can see that at 0.5 s the wind farm voltage drops, and then at 0.6 s it recovers the balance.

Figure 7 shows the waves of the VSC-HVDC system connected to the wind farm under the PI method, including the reactive power wave, the active power wave, the DC voltage wave, and i_d, i_q waves. It can be seen that when the wind farm voltage becomes unbalanced, the reactive power and the active power waves both have major fluctuations. The DC voltage overshoots with the maximum of 3.8 pu at the start, and with unbalanced AC voltage from 0.5 s to 0.6 s, it fluctuates very much; then, until 0.7 s, the DC voltage can track its given

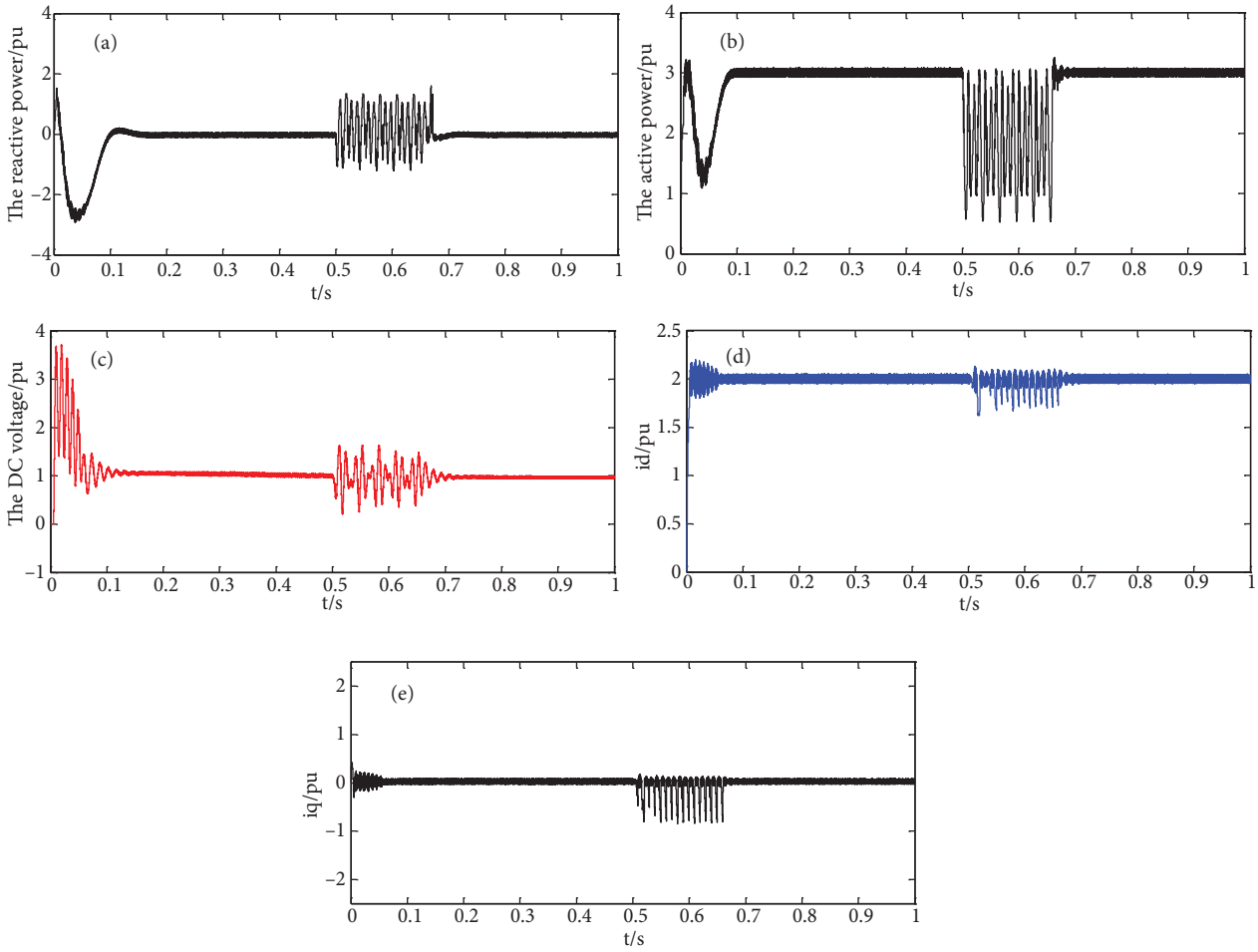

Figure 7. The VSC-HVDC system simulation waves under PI method: (a) reactive power wave (per unit); (b) active power wave (per unit); (c) DC voltage wave (per unit); (d) i_d wave (per unit); (e) i_q wave (per unit).

value with small error. It is also similar to the i_d, i_q waves; that is to say, when the system starts up, i_d and i_q fluctuate; after 0.5 s, they have large fluctuations; and after 0.7 s the system recovers to a steady state.

From Figure 8, it can be easily seen that in the system under the PBC method, before 0.5 s when the wind farm voltages are balanced, the active power is quickly stabilized to 3 pu and the reactive power is stabilized to 0, which indicates that the power factor is 1. i_d is stabilized to 2 pu and i_q is stabilized to 0. The DC voltage is 1 pu with an accepted small error. The dynamic and static performances under the PBC method are good. The decoupled control of the active power and the reactive power is achieved by this method. At 0.5 s, the wind farm voltages become unbalanced, which can be easily seen from Figure 6. Under the proposed method, the system responds fast. The active power and the reactive power fluctuate little and i_d and i_q maintain values of 2 and 0 respectively, as before. The DC voltage tracks its given value and maintains 1 pu with small error. The system with unbalanced voltage has good and stable accuracy and rapid response. After 0.6 s, the wind farm voltage recovers its balance, and it can be seen that the system quickly returns to a stable state. The DC voltage, the active power, and the reactive power become stable rapidly. Thus, it can be seen that the VSC-HVDC system based on the PBC method has rapid recovery capabilities.

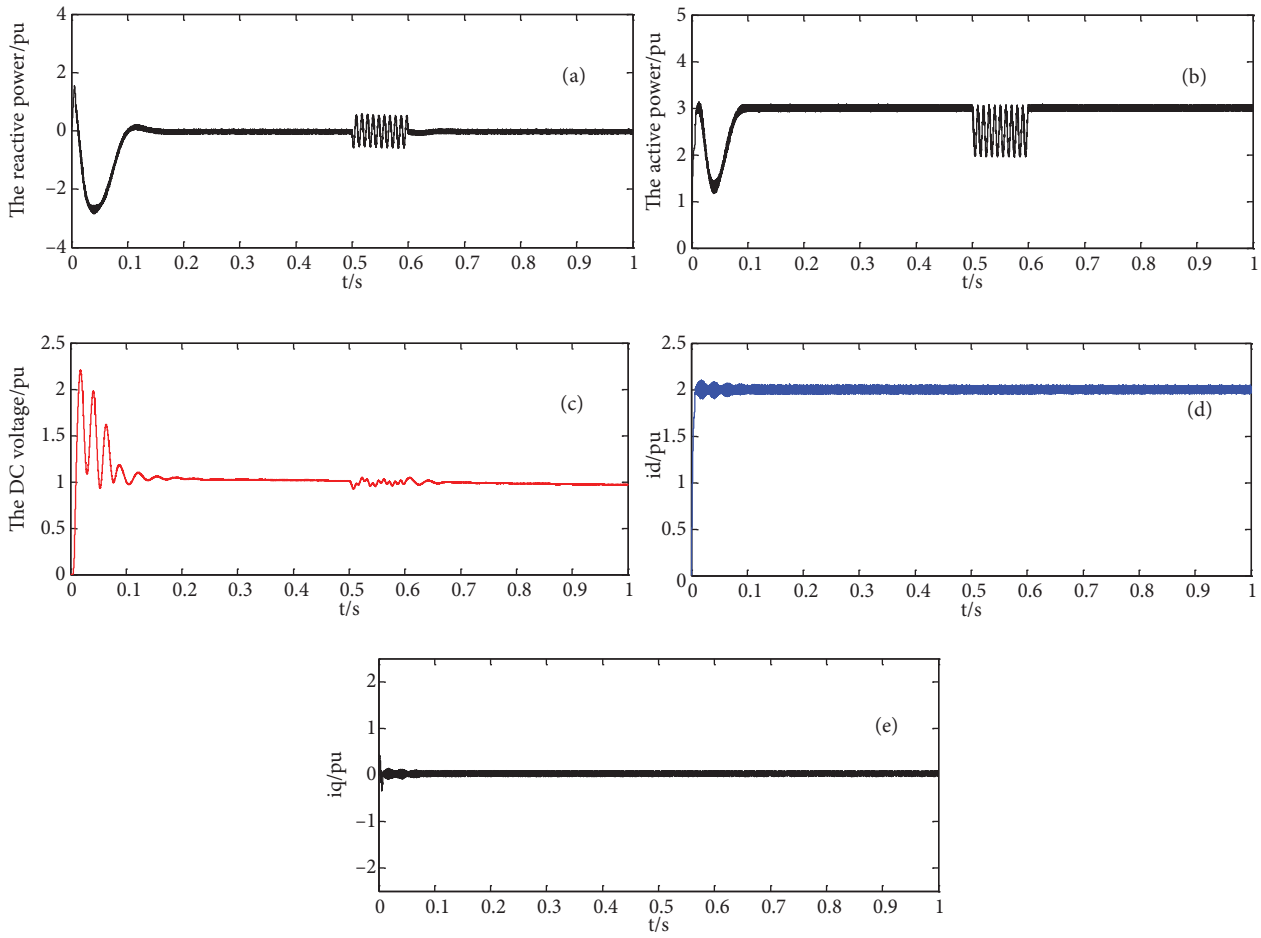

Figure 8. The VSC-HVDC system simulation waves under PBC method: (a) reactive power wave (per unit); (b) active power wave (per unit); (c) DC voltage wave (per unit); (d) i_d wave (per unit); (e) i_q wave (per unit).

By contrasting Figures 7 and 8, we can see that under the PBC method, the system has a faster response and higher steady precision. The dynamic and steady performances are improved. These results indicate the successful implementation of the PBC method. The feasibility and correctness of the method are verified.

6. Conclusion

A PBC method for a VSC-HVDC system in a grid-connected wind farm when the wind farm voltage is unbalanced is proposed in the paper. The mathematical model of VSC with unbalanced voltage was established. The PBC theory was introduced, and then the stability of PBC was proven in light of the Lyapunov stability theory. According to PBC theory, the EL mathematical model of VSC was constructed. The strict passivity of VSC was proven. The control law was deduced in detail. In order to accelerate the convergence speed, dampers were added to the PBC controller.

In order to verify the correctness of the PBC theory in the VSC-HVDC system, a simulation was performed. The simulation model of the VSC-HVDC system based on PBC method was constructed based on MATLAB/SIMULINK. The system under the PI method was also studied. By contrasting the PI method and PBC method, the conclusion was reached that the system under the PBC method has a faster response and higher steady precision, and the decoupled control of the active power and the reactive power was achieved.

The dynamic and steady performances of the VSC-HVDC system when the wind farm voltage is unbalanced were significantly improved. Furthermore, the robustness of the system was enhanced.

Acknowledgment

This paper was supported by the 'Fundamental Research Funds for the Central Universities' (2014MS89).

References

[1] Benchagra M, Maaroufi M, Ouassaid M. A performance comparison of linear and nonlinear control of a SCIG-wind farm connecting to a distribution network. Turk J Electr Eng Co 2014; 22: 1–11.

[2] Bashi MH, Ebrahimi A. Markovian approach applied to reliability modeling of a wind farm. Turk J Electr Eng Co 2014; 22: 287–301.

[3] Fan XM, Guan L, Xia CJ, He JM. Multilevel VSC-HVDC applied in wind power integration. Gaodianya Jishu 2013; 39: 497–504 (article in Chinese with an abstract in English).

[4] Li X, Han MX. A coordinated control strategy of series multi-terminal VSC-HVDC for offshore wind farm. Diangong Jishu Xuebao 2013; 28: 43–57 (article in Chinese with an abstract in English).

[5] Ding YP. The research on HVDC-flexible used in wind farm grid connection. Changsha, China: Changsha University of Science and Technology, 2012 (article in Chinese with an abstract in English).

[6] Ramdan HS, Siguerdidjane H, Petit M, Kaczmarek R. Performance enhancement and robustness assessment of VSC-HVDC transmission systems controllers under uncertainties. Int J Electr Power Energy Syst 2012; 35: 34–36.

[7] Tavana SN, Gharehpetian G, Abedi M, Bidadfar A. Novel control strategy for voltage source converters based on energy function. Turk J Electr Eng Co 2013; 21: 924–933.

[8] Bidadfar A, Abedi M, Karrari M, Gharehpetian GB, Tavana SN. Passive AC network supplying the integration of CCC-HVDC and VSC-HVDC systems. Turk J Electr Eng Co 2014; 22: 353–362.

[9] Asplund G. Application of HVDC light to power system enhancement. In: IEEE 2000 Power Engineering Society Winter Meeting 2000, 23–27 January 2000; Singapore. New York, NY, USA: IEEE. pp. 2498–2503.

[10] Gambino G, Sciacca V. Intermittent and passivity based control strategies for a hyperchaotic system. Appl Math Comput 2013; 221: 367–382.

[11] De R, Anton HJ. Some applications of passivity-based control and invariance principles. IET Control Theory Appl 2013; 7: 1039–1048.

[12] Liu YH, Huo HJ, Chu B, Li C. Passivity-based torque tracking control and adaptive observer design of induction motors. Kong Zhi Li Lun Yu Ying Yong 2013; 8: 1021–1026 (article in Chinese with an abstract in English).

[13] Wang WJ, Chen JY. Passivity-based sliding mode position control for induction motor drives. IEEE Trans Energy Convers 2005; 20: 316–321.

[14] Cheng ZP, Jiao LC. Hamiltonian modeling and passivity-based control of permanent magnet linear synchronous motor. J Comput 2013; 8: 501–508.

[15] Li JY, Liu YH, Wu HL, Chu B. Passivity-based robust control of permanent magnet synchronous motors. J Comput Inf Syst 2013; 9: 4965–4972.